Rotation Curve of the Milky Way out to $\sim$ 200 kpc

Pijushpani Bhattacharjee[1,2,3], Soumini Chaudhury[2,4], and Susmita Kundu[2,5]

ABSTRACT

The rotation curve (RC) of the Galaxy, the Milky Way, is constructed starting from its very inner regions (few hundred pc) out to a large galactocentric distance of $\sim 200\,\mathrm{kpc}$ using kinematical data on a variety of tracer objects moving in the gravitational potential of the Galaxy. We study the effect on the RC due to the uncertainties in the values of the Galactic Constants (GCs) R_0 and V_0 (these being the sun's distance from and circular rotation speed around the Galactic center, respectively) and the velocity anisotropy parameter β of the halo tracer objects used for deriving the RC at large galactocentric distances. The resulting RC in the disk region is found to depend significantly on the choice of the GCs, while the dominant uncertainty in the RC at large distances beyond the stellar disk comes from the uncertainty in the value of β. In general we find that the mean RC steadily declines at distances beyond $\sim 50\,\mathrm{kpc}$. Also, at a given radius, the circular speed is lower for larger values of β (i.e., for more radially biased velocity anisotropy). Considering recent results from large numerical simulations, which find an increasingly radially biased velocity ellipsoid of the Galaxy's stellar population at large distances, with stellar orbits tending to be almost purely radial ($\beta \to 1$) beyond $\sim 100\,\mathrm{kpc}$, our results, for the case of $\beta = 1$, give a model independent estimate of the total mass of the Galaxy within $\sim 200\,\mathrm{kpc}$, $M(200\,\mathrm{kpc}) \gtrsim (6.8 \pm 4.1) \times 10^{11} M_{\odot}$. The complete RC of the Galaxy given here may be useful for deriving the phase space properties of the Galaxy's dark matter halo.

Subject headings: Galaxy: rotation curve – Galaxy: dark matter – Galaxy: mass

[1]McDonnell Center for the Space Sciences & Department of Physics, Washington University in St. Louis, Campus Box 1105, One Brookings Drive, St. Louis, MO 63130. USA.

[2]AstroParticle Physics & Cosmology Division and Centre for AstroParticle Physics, Saha Institute of Nuclear Physics, 1/AF Bidhannagar, Kolkata 700064. India.

[3]E-mail: pijush.bhattacharjee@saha.ac.in

[4]E-mail: soumini.chaudhury@saha.ac.in

[5]E-mail: susmita.kundu@saha.ac.in

1. Introduction

The circular velocity, $V_c(r) = \sqrt{GM(r)/r}$, of a test particle at a radial distance r from the center of a mass distribution gives a direct measure of the total gravitational mass, $M(r)$, contained within that radius. A measured profile of V_c as a function of r for a spiral galaxy — often simply called its Rotation Curve (RC) — is therefore a direct probe of the spatial distribution of the total gravitating mass inside the galaxy including its dark matter (DM) content; see, e.g., Sofue & Rubin (2001), Trimble (1987) for reviews. Recent reviews of using the RC to construct mass models for our Galaxy, the Milky way, can be found, e.g., in Weber & de Boer (2010); Sofue (2012); Nesti & Salucci (2013).

Recently, it has been shown that the RC of the Milky Way can be directly used to derive not only the local density of DM, but also the velocity distribution of the DM particles in the Galaxy (Bhattacharjee et al. 2013), which are crucial for analyzing the results of both direct as well as indirect DM search experiments (Jungman et al. 1996); see also Cowsik et al. (2007); Chaudhury et al. (2010); Kundu & Bhattacharjee (2012); Burch & Cowsik (2013).

The circular velocity of a test particle in the Galaxy is, of course, not a directly measured quantity. The RC of the Galaxy has to be derived from the kinematical as well as positional data for an appropriate set of tracer objects moving in the gravitational field of the Galaxy. Except in few cases, the full 3-D velocity information of the tracers is not available, and the RC has to be reconstructed from only the measured line-of-sight (*los*) velocity and positional information of various tracer objects in the Galaxy.

For deriving the RC in the disk region of the Galaxy, one usually makes the reasonable assumption that the disk tracer objects move in circular orbits around the Galactic center. From the observed heliocentric *los* velocities, $v_{\rm h}$, of the tracers and their position coordinates in the Galaxy, and with an assumed set of values of the Galactic Constants (GCs), $[R_0, V_0]$, where R_0 and V_0 are the sun's distance from and circular rotation speed around the Galactic center, respectively, that define the Local Standard of Rest (LSR) frame, and applying corrections for the peculiar motion of the sun with respect to the LSR, one can obtain the circular velocities around the Galactic center, V_c, in a fairly straightforward manner (Binney & Merrifield 1998). Observations on a variety of tracers such as HI regions, CO emission associated with HII regions, compact objects like Carbon stars (C stars), Cepheids, planetary nebulae (PNe), masers, and so on, have been used to derive the RC of the Galaxy in the disk region. Some recent compilations of RC data for the disk region of the Galaxy can be found, e.g., in Sofue et al. (2009) and Burch & Cowsik (2013).

To derive the RC in the outer regions of the Galaxy beyond the Galactic disk, one has to rely on distant tracers like Blue Horizontal Branch (BHB) stars, K Giant (KG) stars and relatively rare tracer objects like Globular Clusters (GCl), dwarf spheroidal (dSph) galaxies and so forth which populate the Milky Way's extended DM halo out to galactocentric distances of several hundreds of kpc. Unlike the disk tracers, these non-disk tracers do not exhibit any systematic motion, and move about in the Galaxy along various different orbits. The standard approach then is to assume that the tracer population under consideration is isotropically distributed in the halo of the Galaxy and then use the Jeans equation (Binney & Tremaine 2008) for spherical systems relating the circular velocity V_c at radius r to the number density and galactocentric radial as well as transverse velocity dispersions of the tracers at that radius. Of course, in absence of full 3-D velocity information, with only the observed radial velocity dispersion available, the RC constructed using Jeans equation depends on the unknown velocity anisotropy parameter $\beta \equiv 1 - \sigma_t^2/2\sigma_r^2$ (σ_r and σ_t being the radial and transverse velocity dispersions of the tracers, respectively; see section 3 below). However, recent high resolution hydrodynamical simulations of formation of late-type spirals like our Galaxy (Rashkov et al. 2013) are beginning to allow extraction of crucial information on the velocity anisotropy parameter β from comparison of the kinematical properties of the (simulated) halo stars in large mock samples of these objects with observational data. It is, therefore, now possible to go one step further and attempt to construct the RC of the Galaxy to the furthest galactocentric distances possible by using this information.

In this paper we address ourselves to this task and present a RC of the Galaxy spanning a large range of galactocentric distances starting from its inner regions ($\sim 0.2\,\mathrm{kpc}$) out to $\sim 200\,\mathrm{kpc}$, which can be directly used to extract information about the nature of the phase space distribution of the DM particles in the Galaxy.

The Jeans equation approach has been used in several recent studies to extend the RC of the Galaxy to distances beyond the extent of the Galaxy's stellar disk. Accurate measurements of *los* velocities of a sample of 2401 BHB stars drawn from SDSS DR6 (Adelman-McCarthy et al. 2008) were used by Xue et al. (2008) to derive the RC of the Galaxy to $\sim 60\,\mathrm{kpc}$ for two constant (r-independent) values of β, namely $\beta = 0$ (isotropic velocity distribution) and $\beta = 0.37$, the latter derived from results of numerical simulations. More recently, the Jeans equation has also been employed, together with certain analytical models of the phase-space distribution function of the tracer population, to construct the RC of the Galaxy to various distances of ~ 25 to ~ 80 kpc (Gnedin et al. 2010; Deason et al. 2012a; Kafle et al. 2012).

A crucial ingredient in the derivation of the distant RC using Jeans equation is the measured radial velocity dispersion of the tracers as a function of their galactocentric distance r. An important finding in this regard is the result, first shown by Battaglia et al. (2005, 2006), that the radial velocity dispersion remains almost constant at a value of $\sim 120\,\mathrm{km\,s^{-1}}$ out to $\sim 30\,\mathrm{kpc}$ and then steadily *declines* down to a value of $\sim 50\,\mathrm{km\,s^{-1}}$ at $r \sim 120\,\mathrm{kpc}$, implying a declining RC of the Galaxy at distances beyond a few tens of kpc from the center. In their work Battaglia et al. (2005, 2006) used a heterogeneous sample of about 240 halo objects consisting of field blue horizontal branch stars, red giant stars, globular clusters and distant satellite galaxies. Similar trend of the radial velocity dispersion profile has been found in several subsequent studies using different samples of tracers, e.g., by Xue et al. (2008); Brown et al. (2010); Gnedin et al. (2010); Deason et al. (2012a,b), and most recently in large cosmological simulations by Rashkov et al. (2013).

In this paper we consider a combination of currently available largest samples of a variety of both disk and non-disk tracers to construct the RC of the Galaxy from $\sim 0.2\,\mathrm{kpc}$ to $\sim 200\,\mathrm{kpc}$. We perform detailed analysis of the dependence of the RC on the choice of the GCs and also the dependence on the anisotropy parameter β of the non-disk tracers. We find that, while the RC in the disk region is significantly influenced by the choice of the GCs, the dominant uncertainty in the RC at large distances beyond the stellar disk comes from the uncertainty in the value of β. In general, we find that the mean RC steadily declines beyond $r \sim 50\,\mathrm{kpc}$, with lowest values of rotation speeds at large distances obtaining for the case of complete radial anisotropy ($\beta = 1$) of the non-disk tracers. This allows us to set a lower limit on the total mass of the Galaxy, giving $M(\lesssim 200\,\mathrm{kpc}) \geq (6.8 \pm 4.1) \times 10^{11} M_\odot$. The circular speed at a given radius decreases as β is increased (i.e., as the tracers' orbits are made more radially biased). Recent numerical simulation study of Rashkov et al. (2013) indicates an increasingly radially biased velocity ellipsoid of the Galaxy's stellar population at large distances, with stellar orbits becoming purely radial ($\beta \to 1$) beyond $\sim 100\,\mathrm{kpc}$. Thus, the above lower limit on the Galaxy's mass (obtained from our results with $\beta = 1$) may in fact be a good estimate of the actual mass of the Galaxy out to $\sim 200\,\mathrm{kpc}$.

The rest of this paper is arranged as follows. In Section 2 we derive the RC on the disk of the Galaxy up to a distance of $\sim 20\,\mathrm{kpc}$ from the Galactic center. We specify the various tracer samples used in our derivation of the RC and study the dependence of the RC on the chosen set of values of the GCs, $[R_0, V_0]$. In Section 3 we extend the RC to larger distances (up to $\sim 200\,\mathrm{kpc}$) by an extensive analysis of various non-disk tracer samples discussed there in details. Finally, in Section 4, we present our unified RC and our estimates of the total mass of the Galaxy within $\sim 200\,\mathrm{kpc}$ and conclude by summarizing our main results in Section 5.

2. Rotation curve from disk tracers

Let us consider a tracer object with Galactic coordinates (l, b) at a heliocentric distance r_h and observed heliocentric *los* velocity v_h (see Figure 1). We shall assume that the tracer follows a nearly circular orbit about the Galactic center. The velocity of the tracer as would be measured by an observer stationary with respect to the LSR, v_LSR, can be obtained from the measured v_h through the relation

$$v_\mathrm{LSR} = v_\mathrm{h} + U_\odot \cos b \cos l + V_\odot \cos b \sin l + W_\odot \sin b\,, \qquad (1)$$

where $(U_\odot, V_\odot, W_\odot)$ denote the peculiar motion of the sun with respect to LSR; see Figure 1. In our calculations below we shall take $(U_\odot, V_\odot, W_\odot) = (11.1,\ 12.24,\ 7.25)$ ($\mathrm{km\,s^{-1}}$) (Schönrich et al. 2010). Simple algebraic steps then allow us to relate the desired circular velocity with respect to Galactic center rest frame, V_c, to v_LSR as (Binney & Merrifield 1998)

$$V_c(R) = \frac{R}{R_0}\ \left[\frac{v_\mathrm{LSR}}{\sin l \cos b} + V_0\right]\,, \qquad (2)$$

where, R is the projection of the galactocentric distance r onto the equatorial plane,

$$R = \sqrt{R_0^2 + r_\mathrm{h}^2 \cos^2 b - 2R_0\ r_\mathrm{h} \cos b \cos l}\,. \qquad (3)$$

For a given set of GCs, $[R_0, V_0]$, the Cartesian coordinates of the tracer are given by

$$\begin{aligned} x &= r_{\rm h}\ \cos b\ \sin l\,, \\ y &= R_0 - r_{\rm h}\ \cos b\ \cos l\,, \\ z &= r_{\rm h}\ \sin b\,, \end{aligned} \tag{4}$$

with Galactic center at the origin and sun lying on the Galactic mid-plane ($z = 0$) with coordinates $(x, y, z) = (0, R_0, 0)$ as illustrated in the left panel of Figure 1. Hence, for known $(l,\ b,\ r_{\rm h},\ v_{\rm h})$ one can solve for V_c from Equation (2) for a given set of GCs.

Tangent Point Method (TPM) : For $R < R_0$, one can calculate V_c by the simple tangent point method (Binney & Merrifield 1998) as follows: Along a given *los*, the maximum *los* velocity will occur for the tracer closest to the Galactic center, with the *los* tangent to the circular orbit of the tracer at that point (see right panel of Figure 1). This maximum *los* velocity, called the terminal velocity (v_t), is easily seen to be related to V_c through the relation

$$V_c(R_t) = |v_{t,{\rm LSR}}(R_t) + V_0 \sin l|\ , \quad (b = 0)\,, \tag{5}$$

where

$$R_t = |R_0\ \sin l| \tag{6}$$

is the distance of the tangent point from the Galactic center, and $v_{t,{\rm LSR}}$ is the v_t corrected for the sun's peculiar motion as in Equation (1).

For non zero galactic latitude (b), Equation (5) generalizes to:

$$V_c(R_t) = \left|\frac{v_{t,{\rm LSR}}(R_t)}{\cos b} + V_0\ \sin l\right|\,, \tag{7}$$

and in this case the Cartesian coordinates of the tracer are given by

$$\begin{aligned} x &= R_0\ \sin l\ \cos l\,, \\ y &= R_0\ \sin^2 l\,, \\ z &= R_0\ \cos l\ \tan b\,. \end{aligned} \tag{8}$$

Hence the circular velocity V_c can be calculated directly from the measured terminal velocity by using Equation (7).

Table 1 lists the details of the adopted disk tracer samples with corresponding data source references and limits on $l,\ b$ for each tracer genre. The cuts on l and b are adopted from the published source papers. Towards the Galactic center ($l \to 0°$) or anti-center ($l \to 180°$), we expect $v_{\rm LSR}$ to approach zero to prevent unphysical V_c values there [see Equation (2)]. However, $v_{\rm LSR}$ observations in practice have finite values due to contamination from non circular motions dominant there. Therefore, additional restrictions have been applied on l ranges so as to ensure that we avoid observations too close to Galactic center (anti-center) regions. We further impose a cut to keep only the tracers whose $|z| \leq 2\,\mathrm{kpc}$ and $R \leq 25\,\mathrm{kpc}$ so as to ensure that the selected tracers 'belong' to the stellar disk of the Galaxy.

The x–y and l–z scatter plots for the selected disk tracers (as listed in Table 1) are shown in Figure 2 and Figure 3, respectively.

It is clear from Equations (2) – (8) that the RC depends on the set of values of the GCs ($[R_0, V_0]$) adopted in the calculation. Values of R_0 in the range $\sim$ $(7-9)\,\mathrm{kpc}$ and V_0 in the range $\sim$ $(180-250)\,\mathrm{km\,s^{-1}}$ exist in literature (see, e.g., Reid 1993; Olling & Merrifield 1998; Ghez et al. 2008; Reid et al. 2009; McMillan & Binney 2010; Sofue et al. 2011; Brunthaler et al. 2011; Schönrich 2012). Actually, the ratio $V_0/R_0 = (A-B)$, A and B being the Oort constants (see, e.g., Binney & Merrifield 1998), is considerably better constrained. Maser observations and measurements of stellar orbits around SgrA* near the Galactic center report values of $(A-B)$ in the range from about 29 to 32 $\mathrm{km\,s^{-1}\,kpc^{-1}}$ (Reid & Brunthaler 2004; Reid et al. 2009; McMillan & Binney 2010). RCs have been traditionally presented with the IAU recommended set of values, $\left[\frac{R_0}{\mathrm{kpc}}, \frac{V_0}{\mathrm{km\,s^{-1}}}\right]_{\mathrm{IAU}} = [8.5, 220]$, for which, however, the ratio $V_0/R_0 = 25.9$ is outside the range of values of this ratio mentioned above. A recently suggested set of values of $[R_0, V_0]$, consistent with observations of masers and stellar orbits around SgrA* mentioned above, is $\left[\frac{R_0}{\mathrm{kpc}}, \frac{V_0}{\mathrm{km\,s^{-1}}}\right] = [8.3, 244]$ (see, e.g., Bovy et al. 2009; Gillessen et al. 2009).

In general, as easily seen from Equation (2), given a RC, $V_c(R)$, for a certain set of values of $[R_0, V_0]$, one can obtain the new RC, $\tilde{V}_c(R)$, for another set of values of the GCs denoted by $[\tilde{R}_0, \tilde{V}_0]$ through the relation

$$\tilde{V}_c(R) = \frac{R_0}{\tilde{R}_0}\left[V_c(R) - \frac{R}{R_0}\left(V_0 - \tilde{V}_0\right)\right] . \qquad (9)$$

In order to illustrate the dependence of the RC on the choice of the GCs, in this paper we shall calculate RCs with three different sets of values of $\left[\frac{R_0}{\mathrm{kpc}}, \frac{V_0}{\mathrm{km\,s^{-1}}}\right]$, namely the set [8.3, 244] mentioned above as well as two other sets, the IAU recommended set [8.5, 220] and the set [8.0, 200] (Sofue 2012).

Figure 4 shows our calculated RCs for the disk region of the Galaxy. The top panel of Figure 4 shows the RCs for each of the different tracer samples listed in Table 1 for the GCs set $\left[\frac{R_0}{\mathrm{kpc}}, \frac{V_0}{\mathrm{km\,s^{-1}}}\right] = [8.3, 244]$, and the bottom panel shows the RCs obtained by taking the weighted averages of the combined V_c data from all the samples shown in the top panel, for three different sets of values of the GCs as indicated.

The circular velocities and their errors for individual disk tracer samples displayed in the top panel of Figure 4 are obtained in the following way: For each tracer object in a given sample we calculate V_c and R for the object from the known position coordinates of the object and its measured *los* velocity as described above. We then bin the resulting data (V_c vs. R) in R, and in each R bin calculate the mean of all the V_c values of all the objects contained within that bin and assign it to the mean R value of the objects in that bin. The error bars on V_c correspond simply to the standard deviation (s.d.) of the V_c values in that bin [1]. We have taken a bin size of 0.25 kpc for $0 < R \leq 1\,$kpc, 1.0 kpc for $1 < R \leq 15\,$kpc, and 2.5 kpc for $15 < R \leq 17.5\,$kpc. The objects with $R > 17.5\,$kpc are few in number and are placed in one single bin. The above choices of the bin widths in R for various ranges of R, arrived at by trial and error, are "optimal" in the sense that the bin widths are large enough so that there are sufficient number of objects in each bin (to allow the mean value of V_c in the bin to be a reasonably good representative of the true value of V_c at the value of R under consideration), while at the same time being not too large as to miss the fine features of the RC. The RCs in the bottom panel of Figure 4 are obtained by combining the V_c data from all the samples shown in the top panel in the same R bins as above and then calculating the mean circular speed (V_c) and its 1σ uncertainty (ΔV_c) within each bin by the standard weighted average method (Bevington & Robinson 2003):

$$V_c = \frac{\sum_i w_i V_{c,i}}{\sum_i w_i}\,, \quad \text{and} \quad \Delta V_c = \sqrt{\frac{1}{\sum_i w_i}}\,, \tag{10}$$

with $w_i = 1/(\Delta V_{c,i})^2$, where $V_{c,i}$ and $\Delta V_{c,i}$ are the V_c value and its 1σ error, respectively, of the i-th data point within the bin.

As seen from Figure 4, the RC in the disk region depends significantly on the choice of GCs. As expected, at any given R the circular velocity is higher for higher value of V_0.

3. Rotation curve from non-disk tracers

In order to extend the RC beyond the Galactic disk we next consider tracer objects populating the stellar halo of the Galaxy. Unlike the nearly circularly rotating disk tracers the non-disk tracers do not exhibit any systematic circular motion. Hence the formalism described in the previous section cannot be used to derive the RC at large galactocentric distances beyond the Galactic disk. Instead, we use the Jeans equation (see, e.g., Binney & Tremaine 2008, p.349) for spherical systems relating the number density and radial as well as transverse velocity dispersions of the tracers at radius r to the circular velocity V_c at that radius:

$$V_c^2(r) = \frac{GM(r)}{r} = -\sigma_r^2 \left(\frac{d\ln n_{\rm tr}}{d\ln r} + \frac{d\ln \sigma_r^2}{d\ln r} + 2\beta \right)\,. \tag{11}$$

Here $r = \left(R_0^2 + r_{\rm h}^2 - 2R_0\; r_{\rm h} \cos b \cos l\right)^{1/2}$ is the galactocentric radial distance of a tracer (see Figure 1), $n_{\rm tr}$ is the number density of the tracer population at r, σ_r is their galactocentric radial velocity dispersion, and β is the velocity anisotropy parameter defined as,

$$\beta = 1 - \frac{\sigma_t^2}{2\sigma_r^2}\,, \tag{12}$$

[1] Note that the *los* velocities $v_{\rm h}$ of individual tracer objects are measured fairly accurately and their measurement errors contribute negligibly little to the final errors on the V_c values

with σ_t the galactocentric transverse velocity dispersion of the tracers.

In this work we have chosen two independent classes of non-disk stellar tracers, namely, a sample of 4985 Blue Horizontal Branch (BHB) stars from SDSS-DR8 compiled by Xue et al. (2011) and a set of 4781 K Giant (KG) stars from SDSS-DR9 (Xue et al. 2012). These two samples allow us to probe the Galactic halo up to a galactocentric distance of $\sim 100\,\mathrm{kpc}$. In order to reach out further we consider an additional heterogeneous (Hg) sample of 430 objects comprising of 143 Globular Clusters (GCl) (Harris 2010,1996), 118 red halo giants (RHG) (Carney et al. 2003,2008), 108 field blue horizontal branch (FHB) stars (Clewley et al. 2004), 38 RR-Lyrae stars (RRL) (Kinman et al. 2012), and 23 dwarf spheroidals (dSph) (McConnachie 2012). To ensure that the sample comprises of only halo objects, we apply a cut on the z and R coordinates of the tracers, leaving out objects with $r < 25\,\mathrm{kpc}$ in all the non-disk tracer samples mentioned above. After these cuts, we are left with a "BHB" sample of 1457 blue horizontal branch stars, a "KG" sample of 2227 K-giant stars and a "Hg" sample of 65 objects comprising of 16 GCls, 28 FHB stars and 21 dSphs, with which we shall construct our RC for the non-disk region. The last sample allows us to extend the RC to a galactocentric distance of 190 kpc, the mean r of the objects in the furthest radial bin in the Hg sample. The spatial distributions of the three final non-disk tracer samples (after position cuts mentioned above) in terms of x-z, y-z and x-y scatter plots are depicted in Figure 5.

The number density of the tracers, $n_{\rm tr}$, appearing in the Jeans equation (11) is estimated in the following way. We radially bin the objects in a given sample and estimate the tracer density from the star counts in the annular volume of each bin and assign it at the mean radius of the objects contained within that bin. In order to ensure a reasonably good number of objects per bin we adopt a variable bin size increasing with distance. For the BHB sample, a uniform bin size of 2 kpc is used over its entire range of r from 25 to 55 kpc. For the KG samples, the bin widths are 2 kpc for $25\,\mathrm{kpc} < r \leq 55\,\mathrm{kpc}$ and 4 kpc for $55\,\mathrm{kpc} < r \leq 103\,\mathrm{kpc}$; objects with $r > 103\,\mathrm{kpc}$ (up to 110 kpc) are all placed in one single bin. For the Hg sample, because of the relatively small total number (65) of objects, we adopt the following optimal, "object wise" binning in increasing order of the galactocentric distance r of the objects: the first 6 radial bins contain 8 objects in each bin; the next 2 bins contain 6 objects in each bin; and, finally, the remaining 5 objects are placed in one single bin. Uncertainties in the number density estimates are obtained from Poissonian errors on the tracer counts in each bin.

The resulting density estimates for the three samples mentioned above with the GCs set $\left[\frac{R_0}{\mathrm{kpc}}, \frac{V_0}{\mathrm{km\,s^{-1}}}\right] = [8.3, 244]$ are shown in Figure 6, where we also show for comparison (see the top left panel of Figure 6) the tracer densities from some earlier studies that used different tracer samples. Our results are seen to be in reasonably good agreement with those obtained in the previous studies. We then perform power-law fits ($n_{\rm tr}(r) \propto r^{-\gamma}$) to the radial profile of the tracer number density for each of the three samples separately. The resulting best power-law fits are also shown in Figure 6. The values of the parameters of the best power-law fit for each tracer sample are given in Table 2. As seen from Table 2 there is no significant difference in the values of $n_{\rm tr}$ and their power-law fit parameters for the three different sets of GCs.

Next, we have to calculate the galactocentric radial velocity dispersion, σ_r, that appears in the Jeans equation (11), for our non-disk samples. To do this we first transform the observed heliocentric *los* velocity, $v_{\rm h}$, of each individual tracer object to $v_{\rm GSR}$, the velocity that would be measured in the Galactic Standard of Rest (GSR) frame. This is easily done by correcting for the circular motion of the LSR (V_0) and solar peculiar motion with respect to LSR, $(U_\odot, V_\odot, W_\odot)$ (see Figure 1):

$$v_{\rm GSR} = v_{\rm h} + U_\odot \cos b \cos l + V_\odot \cos b \sin l + W_\odot \sin b + V_0 \;\cos b\; \sin l\,. \tag{13}$$

For large samples like the BHB and KG stars described above, we calculate the $v_{\rm GSR}$ for all the individual tracers in the same radial bins as used in the estimation of the tracers' number density described above, calculate their dispersion, $\sigma_{\rm GSR}$, and assign it to the mean radius of all the tracers contained within that bin. The corresponding uncertainty, $\Delta\sigma_{\rm GSR}$, in our estimate of $\sigma_{\rm GSR}$ in each bin is calculated by using the standard formula $\Delta\sigma_{\rm GSR} = \sqrt{1/[2(N-1)]}\sigma_{\rm GSR}$ (Lehmann & Castella 1998; Evans et al. 1993; Graham et al. 1994), where N is the number of objects in the bin.

For the Hg sample, however, owing to its small size, we follow a different method, similar to that used in Battaglia et al. (2005, 2006), for calculating the $\sigma_{\rm GSR}$ and its uncertainty in each radial bin: we randomly generate a sample of 10,000 mock values of $v_{\rm h}$ for each tracer object in a radial bin using a Gaussian centered at the observed value of $v_{\rm h}$ and a width of typically $\sim (10-20)\%$ of this $v_{\rm h}$ value. We then transform these 10,000 $v_{\rm h}$ values for each tracer in the bin to get the corresponding 10,000 values of $v_{\rm GSR}$ using equation (13), and calculate the associated dispersion $\sigma_{\rm GSR}$ for each tracer in that bin. We assign the mean value of the $\sigma_{\rm GSR}$ values for all the objects in a given bin to the mean radius of all the objects in the bin. The corresponding uncertainty in $\sigma_{\rm GSR}$ is taken to be the r.m.s. deviation of the $\sigma_{\rm GSR}$ values in that bin.

Our results for $\sigma_{\rm GSR}$ for the three tracer samples are shown in Figure 7 in which we also show for comparison (see the top left panel of Figure 7) the $\sigma_{\rm GSR}$ values obtained in some earlier studies using different samples, which, again, are seen to be in reasonably good agreement with our results. The other three panels of Figure 7 show the best power-law fits ($\sigma_{\rm GSR}(r) \propto r^{-\alpha}$) to the radial profiles of $\sigma_{\rm GSR}$ for each of the three non-disk samples. The values of the parameters of the best power-law fits for the three tracer samples are given in Table 2. Again, as in the case of $n_{\rm tr}$, the effect of variation of the Galactic Constants on $\sigma_{\rm GSR}$ is negligible.

Finally, the galactocentric radial velocity dispersion, σ_r, can be obtained from $\sigma_{\rm GSR}$ by using the relation (Battaglia et al. 2005, 2006)

$$\sigma_r = \frac{\sigma_{\rm GSR}}{\sqrt{1-\beta H(r)}}\,, \tag{14}$$

where

$$H(r) = \frac{r^2+R_0^2}{4r^2} - \frac{\left(r^2-R_0^2\right)^2}{8r^3 R_0}\ln\frac{r+R_0}{r-R_0}\,, \qquad (r > R_0) \tag{15}$$

and β is the velocity anisotropy of the tracers defined in equation (12). Equation (15) is derived by decomposing the $v_{\rm GSR}$'s into their galactocentric radial and transverse components and taking the averages of the squares of the velocity components.[2]

The last quantity that remains to be specified before we can solve the Jeans equation (11) is the velocity anisotropy parameter, β, of the tracers. There is not much definite observational information available on the value of β of the tracers because of the lack of availability of proper motion measurements on sufficiently large number of tracer objects. In general β can be a function of r. A recent maximum likelihood analysis (Deason et al. 2012a) of radial velocity data of a large sample of halo stars, performed within the context of a model for the (in general anisotropic) velocity distribution function of the halo stars, indicates the stellar velocity anisotropy being radially biased with a value of $\beta \sim 0.5$ for r from ~ 16 kpc up to $r \sim 48\,\mathrm{kpc}$. This is also supported by recent results from a large numerical simulation study (Rashkov et al. 2013), which finds that the velocity distribution of the Galaxy's stellar population at large r is indeed radially biased ($\beta > 0$) with stellar orbits tending to purely radial ($\beta \to 1$) at $r \gtrsim 100\,\mathrm{kpc}$. Based on these considerations, in this paper we shall calculate our RCs assuming three representative constant values of β, namely, $\beta = 0$ (isotropic), 0.5 (mildly radially biased anisotropy), and 1 (fully radially anisotropic). We shall also calculate the RC for a radially varying β with the radial profile of β extracted from the results of numerical simulations given in Rashkov et al. (2013).

With $n_{\rm tr}$, σ_r and β thus specified, we can now proceed to solve the Jeans equation (11) to obtain the V_c profiles for the three different tracer samples described above. For each tracer sample we calculate the V_c's in the same radial bins as used in calculating the $n_{\rm tr}$'s and $\sigma_{\rm GSR}$'s, and the best-fit power-law forms of $n_{\rm tr}$ and $\sigma_{\rm GSR}$ described above are used for calculating the radial derivatives appearing in the Jeans equation (11). The corresponding 1σ error, ΔV_c, on V_c within each radial bin is calculated from those of $n_{\rm tr}$ and $\sigma_{\rm GSR}$ in the bin by standard quadrature.

The resulting RCs for the three tracer samples are shown in Figure 8. It is seen that all the RCs are declining beyond $\sim 50\,\mathrm{kpc}$. The declining trend is particularly clear for the KG and Hg samples. Also, as clear from the left panels of Figure 8 the RCs for different choices of GCs almost overlap, thus indicating that the the RC at large galactocentric distances beyond a few tens of kpc is fairly insensitive to (our lack of) precise knowledge of the GCs. Instead, the main uncertainty in the RC comes from the unknown value of the tracers' velocity anisotropy parameter β. As expected, the lowest rotation speeds obtain for the most radially biased velocity anisotropy ($\beta = 1$).

4. Combined rotation curves to $r \sim 200\,\mathrm{kpc}$

We now combine the rotation curves obtained from disk and non-disk tracers (Figures 4 and 8) to construct the rotation curve of the Galaxy up to $\sim 200\,\mathrm{kpc}$. For the disk region ($r < 25\,\mathrm{kpc}$) we take the V_c data for a chosen set of GCs from the lower panel of Figure 4. For the non-disk

[2] Note that equation (3) given in the 2005 paper of Battaglia et al. (2005, 2006) is incorrect. The correct equation, same as equation (15) above, is given in the 2006 (Erratum) paper of Battaglia et al. (2005, 2006).

region ($r \geq 25\,\mathrm{kpc}$), we combine the V_c data from Figure 8 for the three tracer samples in every 2 kpc radial bins and calculate the resulting mean circular speed (V_c) and its 1σ uncertainty (ΔV_c) within a bin by weighted averaging as described in section 2 [see equation (10)].

The resulting rotation curves for $\beta = 0$ and three sets of values of the GCs are shown in Figure 9, and those for different values of β, for one particular set of GCs, $\left[\frac{R_0}{\mathrm{kpc}}, \frac{V_0}{\mathrm{km\,s^{-1}}}\right] = [8.3, 244]$, are shown in Figure 10. For comparison, we also show in Figure 10 estimates of circular velocities at specific values of r obtained from a variety of independent considerations in some earlier studies by various authors.

The β dependence of the radial profile of the cumulative mass, $M(r) = rV_c^2(r)/G$, is shown in Figure 11. Note that the lowest mass of the Galaxy corresponds to $\beta = 1$, which allows us to set a lower limit on the mass of the Galaxy, $M(\sim 200\,\mathrm{kpc}) \geq (6.8 \pm 4.1) \times 10^{11} M_\odot$.

Finally, the full rotation curve of the Galaxy from its inner region ($r \sim 0.2\,\mathrm{kpc}$) out to $\sim 200\,\mathrm{kpc}$ with $\left[\frac{R_0}{\mathrm{kpc}}, \frac{V_0}{\mathrm{km\,s^{-1}}}\right] = [8.3, 244]$ and for a radial profile of the non-disk tracers' velocity anisotropy parameter β extracted from Figure 2 of Rashkov et al. (2013) is shown in Figure 12.

As already mentioned, a noticeable feature of the rotation curve, irrespective of the velocity anisotropy of the tracer objects, is it's clearly declining nature beyond about ∼50 kpc, as would be expected of an effectively finite size of the dark matter halo of the Galaxy.

We emphasize that, for any given β, the rotation curve and mass profile of the Galaxy shown in Figures 10 and 11, respectively, are based entirely on observational data, and are obtained without making any models of the mass distributions of the various components (the bulge, disk and dark matter halo) of the Galaxy.

5. Summary

In this paper, we have constructed the rotation curve (RC) of the Galaxy from a galactocentric distance of $\sim 0.2\,\mathrm{kpc}$ out to $\sim 200\,\mathrm{kpc}$ by using kinematical data on a variety of both disk and non-disk objects that trace the gravitational potential of the Galaxy. We have studied the dependence of the RC on the choice of the Galactic constants (GCs) and also studied the dependence on the velocity anisotropy parameter β of the non-disk tracers. The RC in the disk region is found to depend significantly on the choice of values of the GCs. The rotation curve at large distances beyond the stellar disk, however, depends more significantly on the parameter β than on the values of the GCs. In general, the mean RC is found to steadily decline beyond $r \sim 50\,\mathrm{kpc}$, irrespective of the value of β. At any given galactocentric distance r, the circular speed is lower for larger values of β. Considering that the largest allowed value of β is unity (complete radial anisotropy), this allows us to set a lower limit on the total mass of the Galaxy, giving $M(\lesssim 200\,\mathrm{kpc}) \geq (6.8 \pm 4.1) \times 10^{11} M_\odot$. We have also noted that recent results from high resolution hydrodynamical simulations of formation of galaxies like Milky Way (Rashkov et al. 2013) indicate an increasingly radially biased velocity ellipsoid of the Galaxy's stellar population at large distances, with stellar orbits tending to be almost purely radial ($\beta \to 1$) beyond $\sim 100\,\mathrm{kpc}$. This implies that the above lower limit on the Galaxy's mass (obtained from our results with $\beta = 1$) may in fact be a good estimate of the actual mass of the Galaxy out to $\sim 200\,\mathrm{kpc}$. We have also given the RC of the Galaxy for a radial profile of β obtained from the results of the numerical simulations of Rashkov et al. (2013), which may be useful for realistic modeling of the phase space properties of the dark matter halo of the Galaxy.

Acknowledgments: We thank G. Battaglia, W. Brown, A. Deason, O. Gnedin, P. Kafle, S. Sharma, Y. Sofue, M. Weber, and X. Xue for useful communications. PB thanks R. Cowsik for discussions and for support under a Clark Way Harrison Visiting Professorship at the McDonnell Center for the Space Sciences and Physics Department at Washington University in St. Louis.

REFERENCES

Adelman-McCarthy, J. K., et al. 2008, ApJS, 175, 297

Battaglia, G., et al. 2005, MNRAS, 364, 433; 2006, MNRAS, 370, 1055 (Erratum)

Battinelli, P., et al. 2012, arXiv:1212.1116

Bevington, P.R., & Robinson, D.K. 2003, Data reduction and error analysis for the physical sciences, 3rd Ed. (New York, NY: McGraw-Hill)

Bhattacharjee, P., et al. 2013, Phys. Rev. D, 87, 083525

Binney, J., & Merrifield, M. 1998, Galactic Astronomy (Princeton, NJ: Princeton Univ. Press)

Binney, J., & Tremaine, S. 2008, Galactic Dynamics (2nd Ed.) (Princeton, NJ: Princeton Univ. Press)

Bond, N. A., et al. 2010, ApJ, 716, 1

Bovy, J., Hogg, D.W., & Hans-Walter, R. 2009, ApJ, 704, 1704

Brand, J., & Blitz, L. 1993, A&A, 275, 67

Brown, W.R., et al. 2010, AJ, 139, 59

Brunthaler, A., et al. 2011, AN, 332, 461

Burch, B., & Cowsik, R. 2013, arXiv:1306.1920

Burton, W. B., & Gordon, M. A. 1978, A&A, 63, 7

Carney, B. W., et al. 2003, AJ, 125, 293; 2008, AJ, 135, 196

Chaudhury, S., Bhattacharjee, P., & Cowsik, R. 2010, J. Cosmology Astropart. Phys., 09, 020

Clemens, D. P. 1985, ApJ, 295, 422

Clewley, L., et al. 2004, MNRAS, 352, 285

Cowsik, R., et al. 2007, New A, 12, 507

Deason, A.J., et al. 2012, MNRAS, 424, L44 [D12a]

Deason, A. J., et al. 2012, MNRAS, 425, 2840 [D12b]

Dehnen, W., & Binney, J. 1998, MNRAS 294, 429

Demers, S. & Battinelli, P. 2007, A&A, 473, 143

Dias, W. S., et al. 2002, A&A, 389, 871

Durand, S., Acker, A., & Zijlstra, A. 1998, A&AS, 132, 13

Evans, M., Hastings, N., & Peacock, B. 1993, Statistical distributions (Wiley, New York)

Fich, M., Blitz, L., & Stark, A. A. 1989, ApJ, 342, 272

Frinchaboy, P. M., & Majewski, S. R. 2008, AJ, 136, 118

Ghez, A. M., et al. 2008, ApJ, 689, 1044

Gillessen, S., et al. 2009, ApJ. 692, 1075

Gnedin, O.Y., et al. 2010, ApJ, 720, L108

Graham, R. L., Knuth, D. E., & Patashnik, O. 1994, Concrete mathematics: A foundation for computer science (Addison-Wesley, Reading)

Harris, W.E. 2010, arXiv:1012.3224; 1996, AJ, 112, 1487

Honma, M., et al. 2007, PASJ, 59, 839

Hou, L. G., Han, J. L., & Shi, W. B. 2009, A&A, 499, 473

Jungman, G., Kamionkowski, M., & Greist, K. 1996, Phys. Rep., 267, 195

Kafle, P.R., et al. 2012, ApJ, 761, 98

Kinman, T. D., et al. 2012, MNRAS, 422, 2116

Kundu, S., & Bhattacharjee, P. 2012, Phys. Rev. D, 85, 123533

Lehmann, E. L., & Casella, G. 1998, Theory of point estimation (Springer-Verlag, New York)

Maciel, W. J. 1984, A&AS, 55, 253

Maciel, W. J., & Lago, L. G. 2005, RMxAA, 41, 383

McConnachie, A. W. 2012, arXiv:1204.1562

McMillan, P. J. 2011, MNRAS, 414, 2446

McMillan, P. J., & Binney, J. 2010, MNRAS, 402, 934

Nesti, F., & Salucci, P. 2013, arXiv:1304.5127

Olling, R. P., & Merrifield, M. R. 1998, MNRAS, 297, 943

Pont, F., Mayor, M., & Burki, G. 1994, A&A, 285, 415

Rashkov, V., et al. 2013, arXiv:1307.1865

Reid, M. J. 1993, ARA&A, 31, 345

Reid, M. J., et al. 2009, ApJ, 700, 137

Reid, M. J., & Brunthaler, A. 2004, ApJ, 616, 872

Samurovic, S., et al. 2011, A&A, 531, A82

Schönrich, R. 2012, MNRAS, 427, 274

Schönrich, R., Binney, J., & Dehnen, W. 2010, MNRAS, 403, 1829

Smith, M. C., Evans, N. W., Belokurov, V., et al. 2009, MNRAS, 399, 1223

Sofue, Y., & Rubin, V. 2001, ARA&A, 39, 137

Sofue, Y., Honma, M., & Omodaka, T. 2009, PASJ, 61, 227

Sofue, Y., et al. 2011, arXiv:1105.1219

Sofue, Y. 2012, PASJ, 64, 75

Trimble, V. 1987, 25, 425

Urquhart, J. S., et al. 2011, arXiv:1111.1625

Watkins, L. L., et al. 2010, MNRAS, 406, 264

Weber, M., & de Boer, W. 2010, A&A, 509, A25

Westerhout, G. 1976, Maryland-Bonn Galactic 21-cm Line Survey, University of Maryland, College Park.

Wilkinson, M. I., & Evans, N. W. 1999, MNRAS, 310, 645

Xue, X.X., et al. 2008, ApJ, 684, 1143

Xue, X. X., et al. 2011, ApJ, 738, 79

Xue, X. X., et. al. 2012, arXiv:1211.0549

This preprint was prepared with the AAS LaTeX macros v5.2.

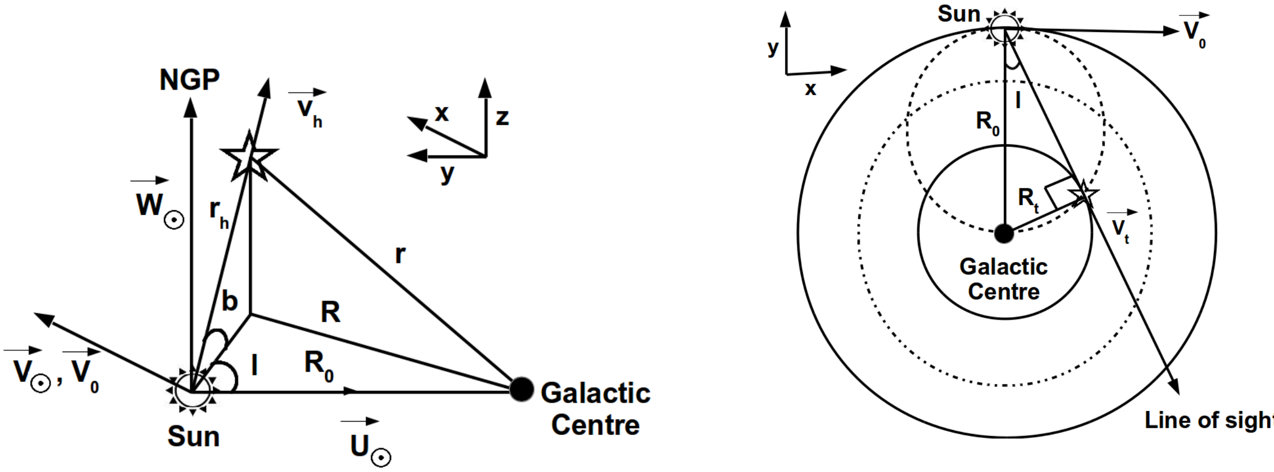

Fig. 1.— Left: Schematic diagram showing the coordinate system, velocity and distance notations used in this work. Right: Illustration of the tangent point method for deriving the circular speeds for distances $R < R_0$ on the disk.

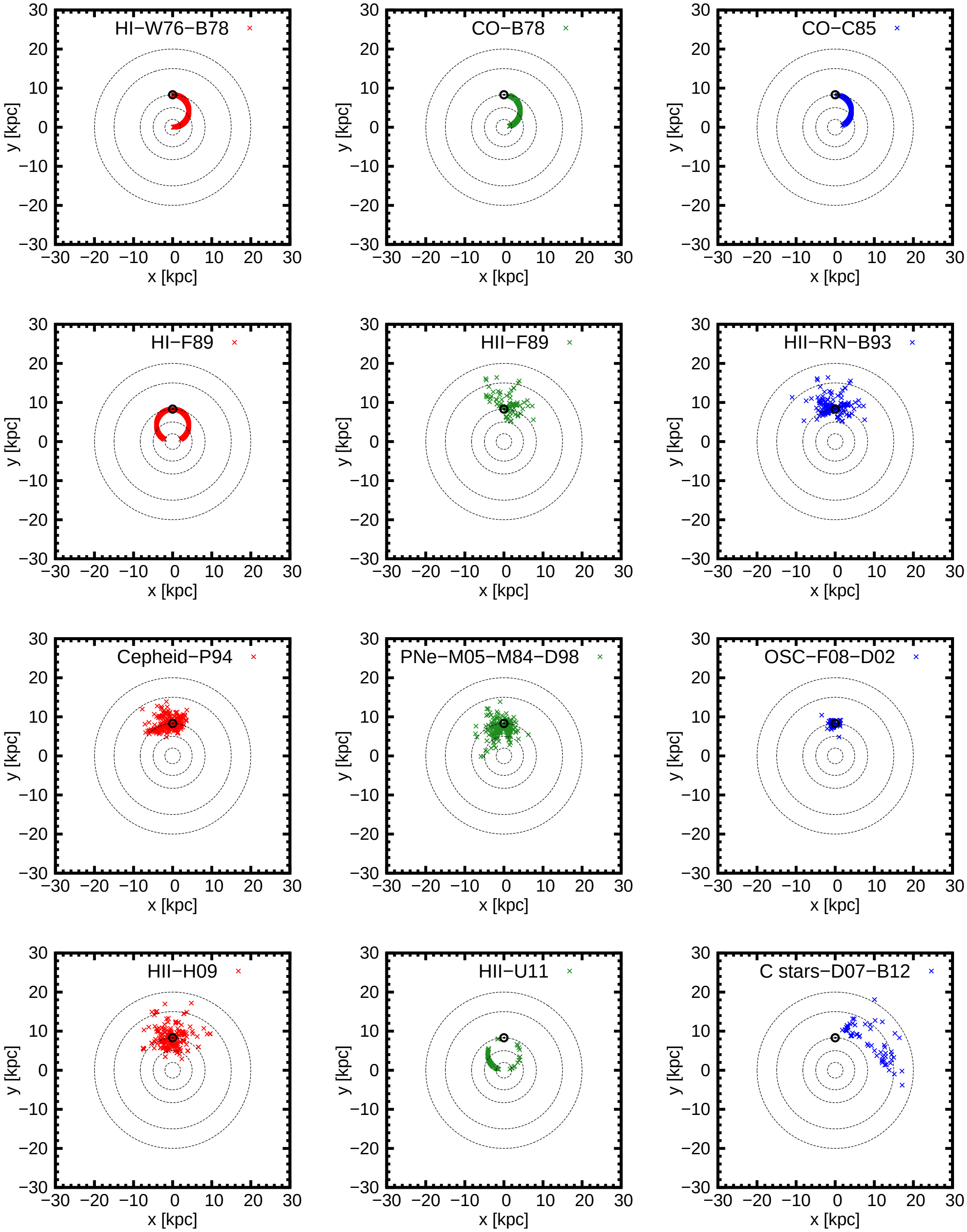

Fig. 2.— x–y scatter plots for the different disk tracer samples listed in Table 1, for the case $R_0 = 8.3\,\mathrm{kpc}$. The Galactic Center is chosen to be at origin $(0, 0)$ with the sun located at $(0, R_0)$.

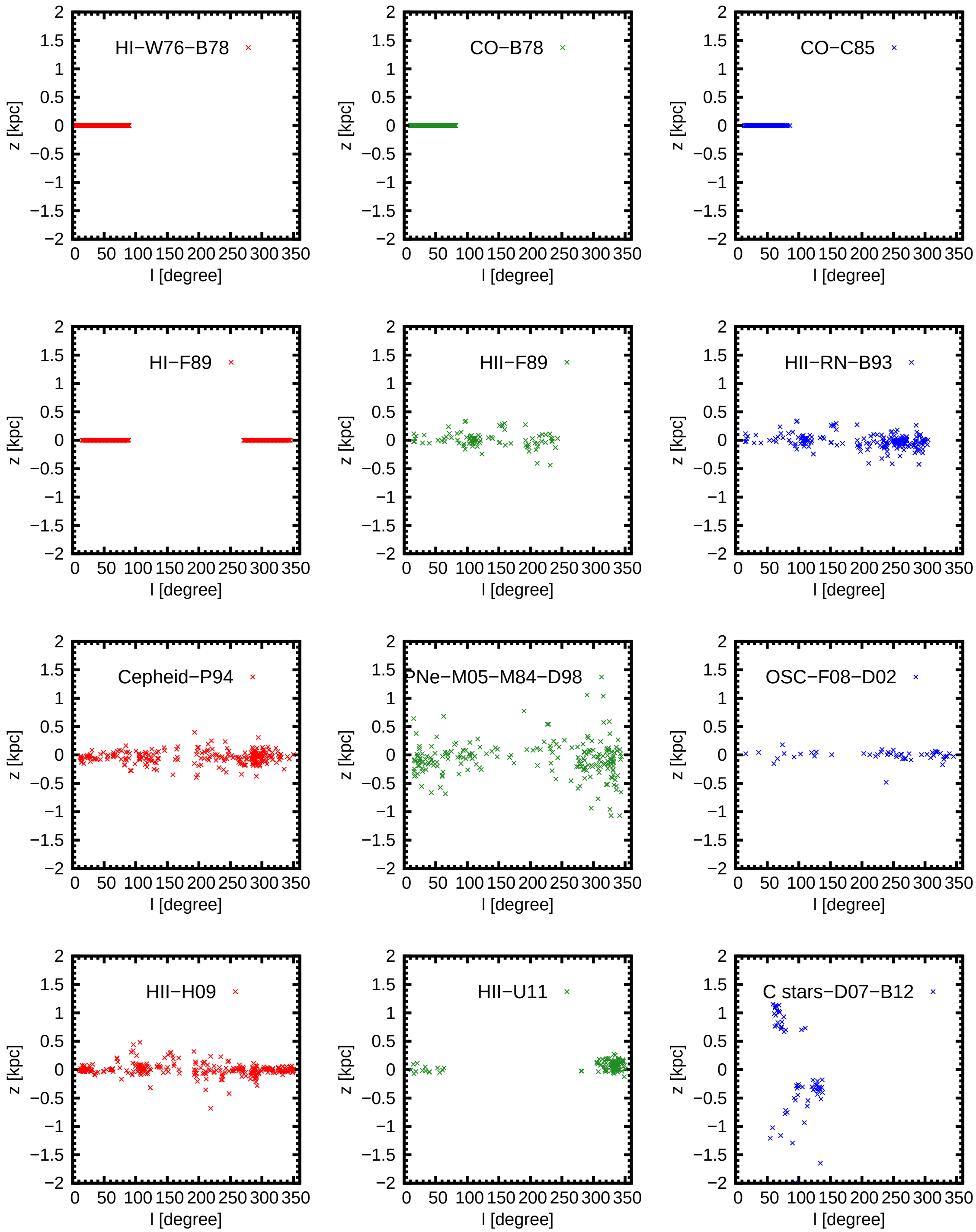

Fig. 3.— Galactic longitude, l (x-axis), versus height from Galactic mid-plane, z (y-axis), for the different disk tracer samples listed in Table 1, for the case $R_0 = 8.3\,\mathrm{kpc}$.

Table 1: Disk tracer types, their source references and $(l,\ b)$ ranges of the data sets used in this paper. Superscript 'a' denotes the tracers limited within the solar circle ($R < R_0$) where tangent point method has been used to derive the rotation speeds. The identifier for each tracer data set used in the paper is given within parentheses in the first column under the respective tracer type for subsequent references in the paper.

Tracer Type	Data Source	(l, b) Ranges
HI regions^a (HI-W76-B78)	Westerhout (1976); Burton & Gordon (1978)	$1^\circ < l < 90^\circ$
CO clouds^a (CO-B78)	Burton & Gordon (1978)	$9^\circ < l < 82^\circ$
CO clouds^a (CO-C85)	Clemens (1985)	$13^\circ < l < 86^\circ$
HI regions^a (HI-F89)	Fich et al. (1989)	$15^\circ < l < 89^\circ$ and $271^\circ < l < 345^\circ$
HII regions (HII-F89)	Fich et al. (1989)	$10^\circ < l < 170^\circ$ and $190^\circ < l < 350^\circ$
HII regions & reflection nebulae (HII-RN-B93)	Brand & Blitz (1993)	$10^\circ < l < 170^\circ$ and $190^\circ < l < 350^\circ$
Cepheids (Cepheid-P94)	Pont et al. (1994)	$10^\circ < l < 170^\circ$ and $190^\circ < l < 350^\circ$; $\|b\| < 10^\circ$
Planetary nebulae (PNe-M05-M84-D98)	Maciel & Lago (2005); Maciel (1984); Durand et al. (1998)	$15^\circ < l < 345^\circ$; $\|b\| < 10^\circ$
Open star clusters (OSC-F08-D02)	Frinchaboy & Majewski (2008); Dias et al. (2002)	$10^\circ < l < 170^\circ$ and $190^\circ < l < 350^\circ$; $\|b\| < 9^\circ$
HII regions (HII-H09)	Hou et al. (2009)	$10^\circ < l < 170^\circ$ and $190^\circ < l < 350^\circ$
HII regions^a (HII-U11)	Urquhart et al. (2011)	$10^\circ < l < 65^\circ$ and $280^\circ < l < 350^\circ$
C stars (C stars-D07-B12)	Demers & Battinelli (2007); Battinelli et al. (2012)	$54^\circ < l < 150^\circ$; $3^\circ < \|b\| < 9^\circ$

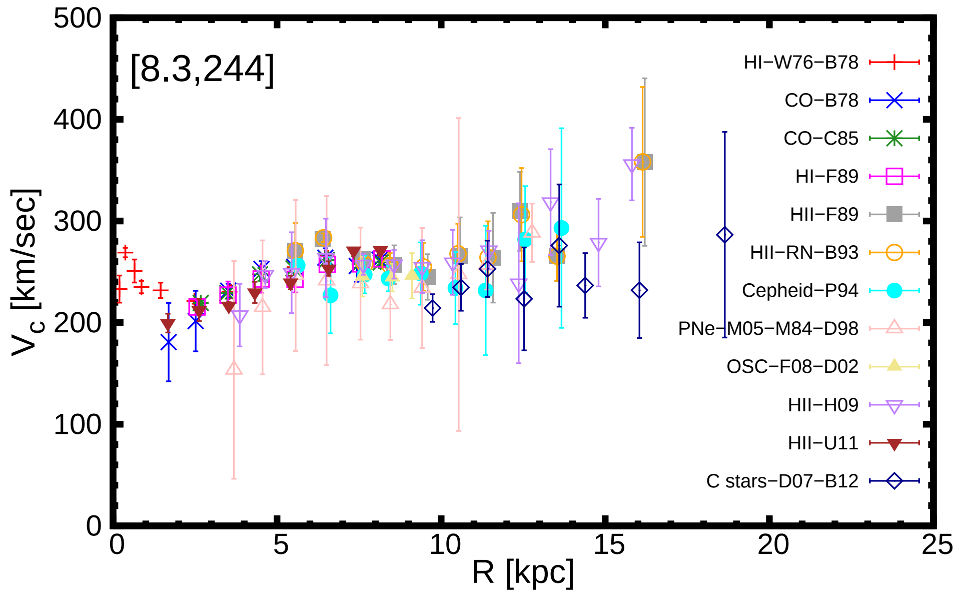

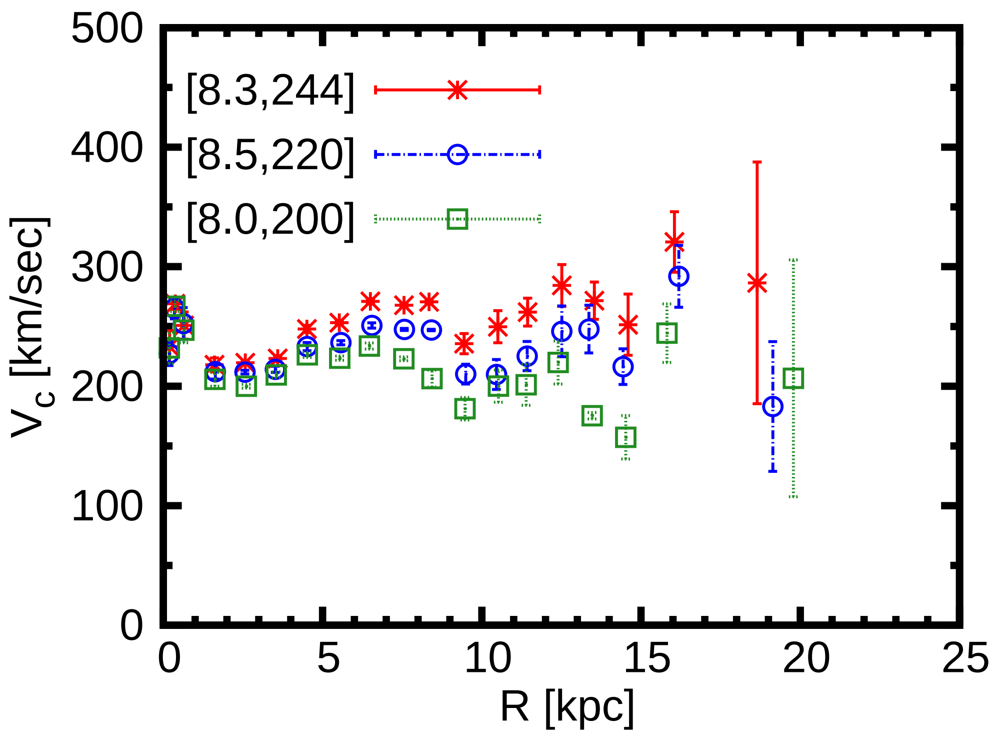

Fig. 4.— Top: Rotation curves of the Galaxy obtained using the various different disk tracer samples listed in Table 1 for the Galactic Constants $\left[\frac{R_0}{\mathrm{kpc}}, \frac{V_0}{\mathrm{km\,s^{-1}}}\right] = [8.3, 244]$. See Table 1 for keys to the data points. Bottom: Averaged rotation curves obtained by weighted averaging over the combined V_c data from all the disk tracer samples listed in Table 1 and shown in the top panel above, for three different sets of values of $\left[\frac{R_0}{\mathrm{kpc}}, \frac{V_0}{\mathrm{km\,s^{-1}}}\right]$ as indicated.

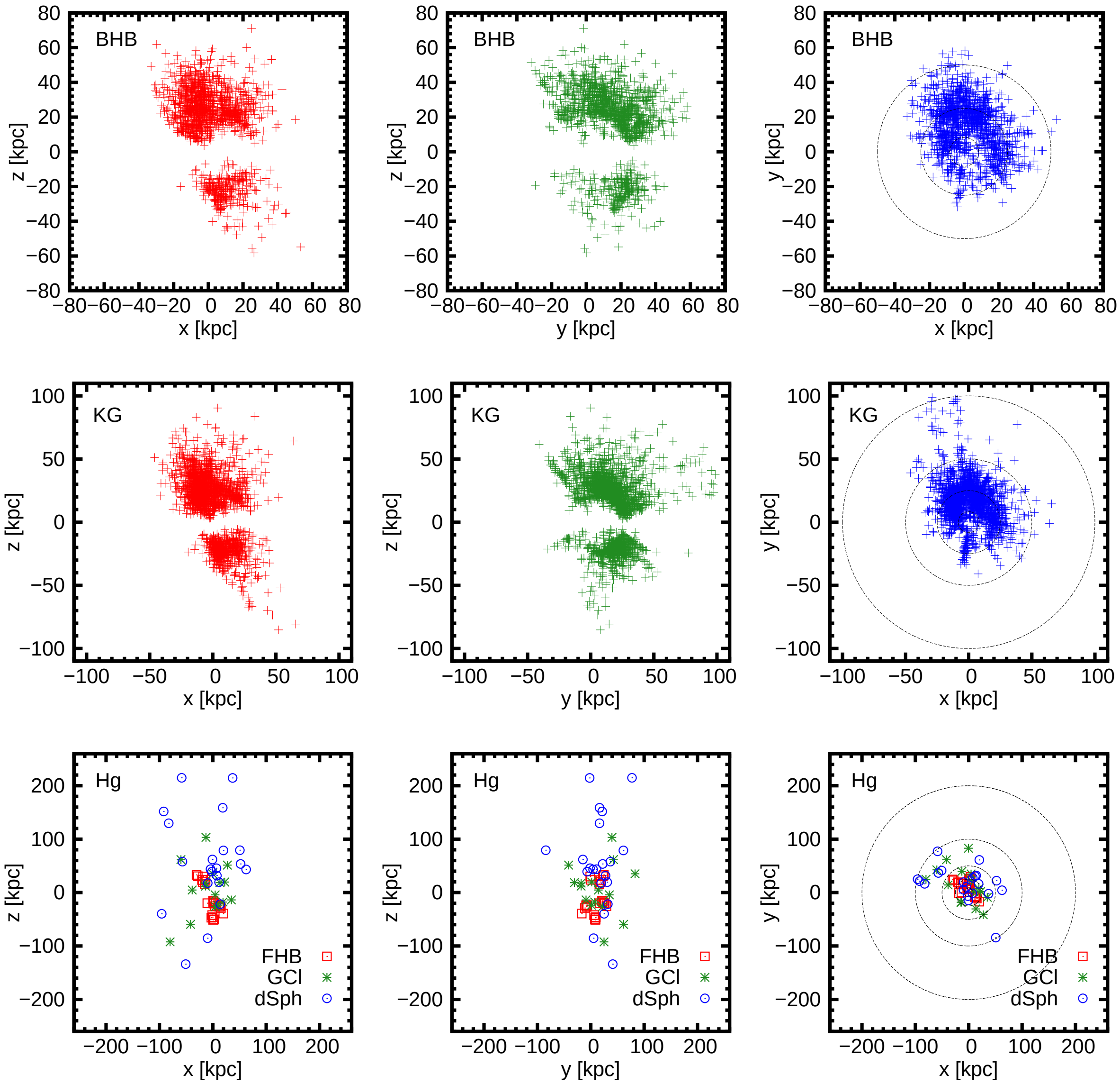

Fig. 5.— x-z, y-z and x-y scatter plots (after removing objects with $r < 25\,\mathrm{kpc}$; see text) for the three samples of non-disk tracer objects considered in this paper, namely, (1) the "BHB" sample, a set of 1457 blue horizontal branch stars from the compilation of Xue et al. (2011), (2) the "KG" sample, a set of 2227 K-Giant stars from the compilation of Xue et al. (2012), and (3) the "Hg" sample, a heterogeneous set of 65 objects comprising of 16 Globular Clusters (GCl) from Harris (2010,1996), 28 field blue horizontal branch (FHB) stars from Clewley et al. (2004), and 28 dwarf spheroidals (dSph) from McConnachie (2012), for $R_0 = 8.3\,\mathrm{kpc}$ with the sun located at $(x = 0, y = R_0, z = 0)$.

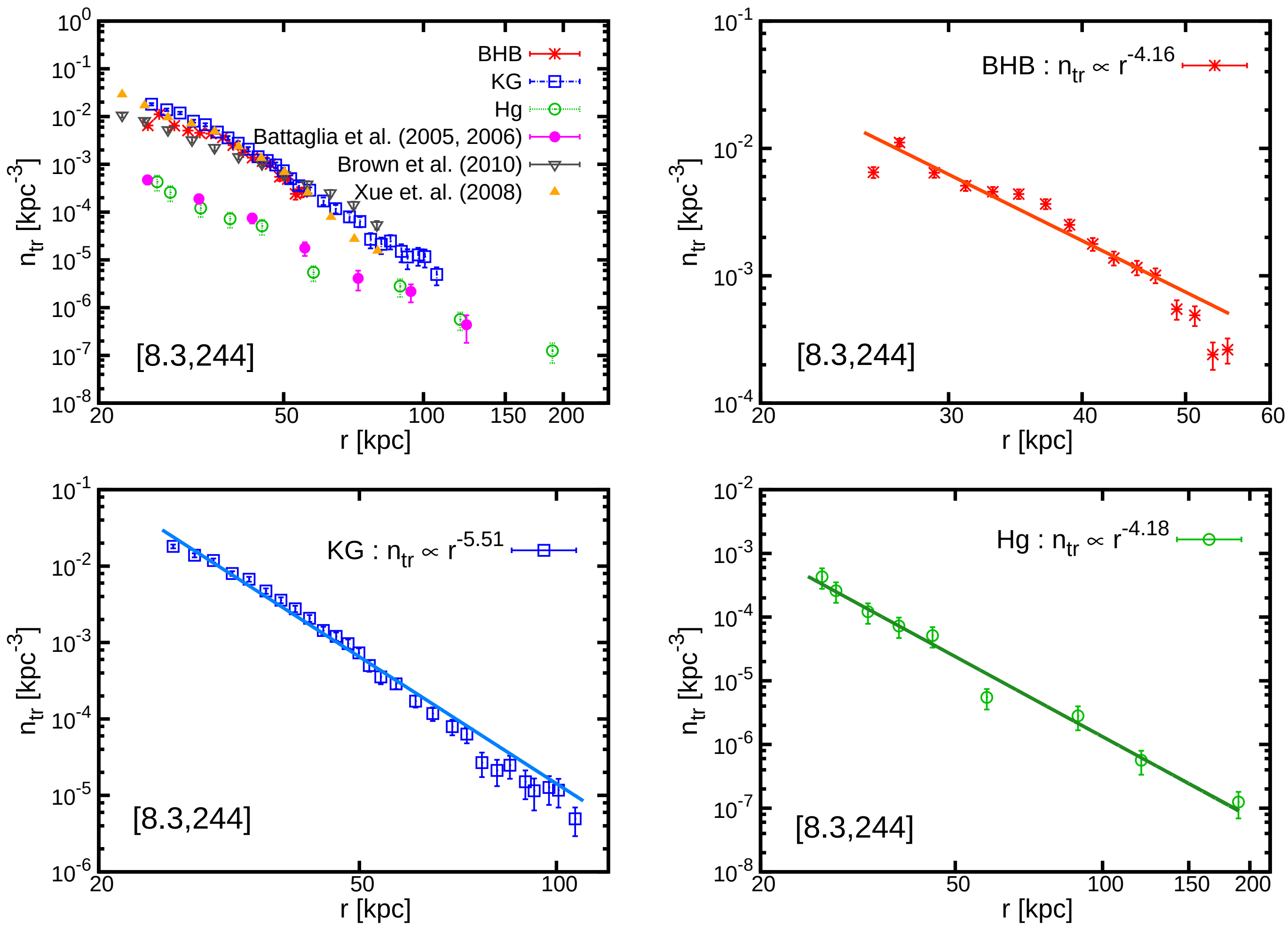

Fig. 6.— The tracer number density, $n_{\rm tr}$, for the three non-disk tracer samples considered in this paper (see text and Figure 5 for details and source references for the samples). The top left panel shows, for comparison, the tracer densities obtained in some earlier studies (Xue et al. 2008; Brown et al. 2010; Battaglia et al. 2005, 2006) which used different tracer samples. The other three panels show the best power law fits to the radial profiles of $n_{\rm tr}$ for the three non-disk samples. The GC set used is $\left[\frac{R_0}{\rm kpc}, \frac{V_0}{\rm km\,s^{-1}}\right] = [8.3, 244]$.

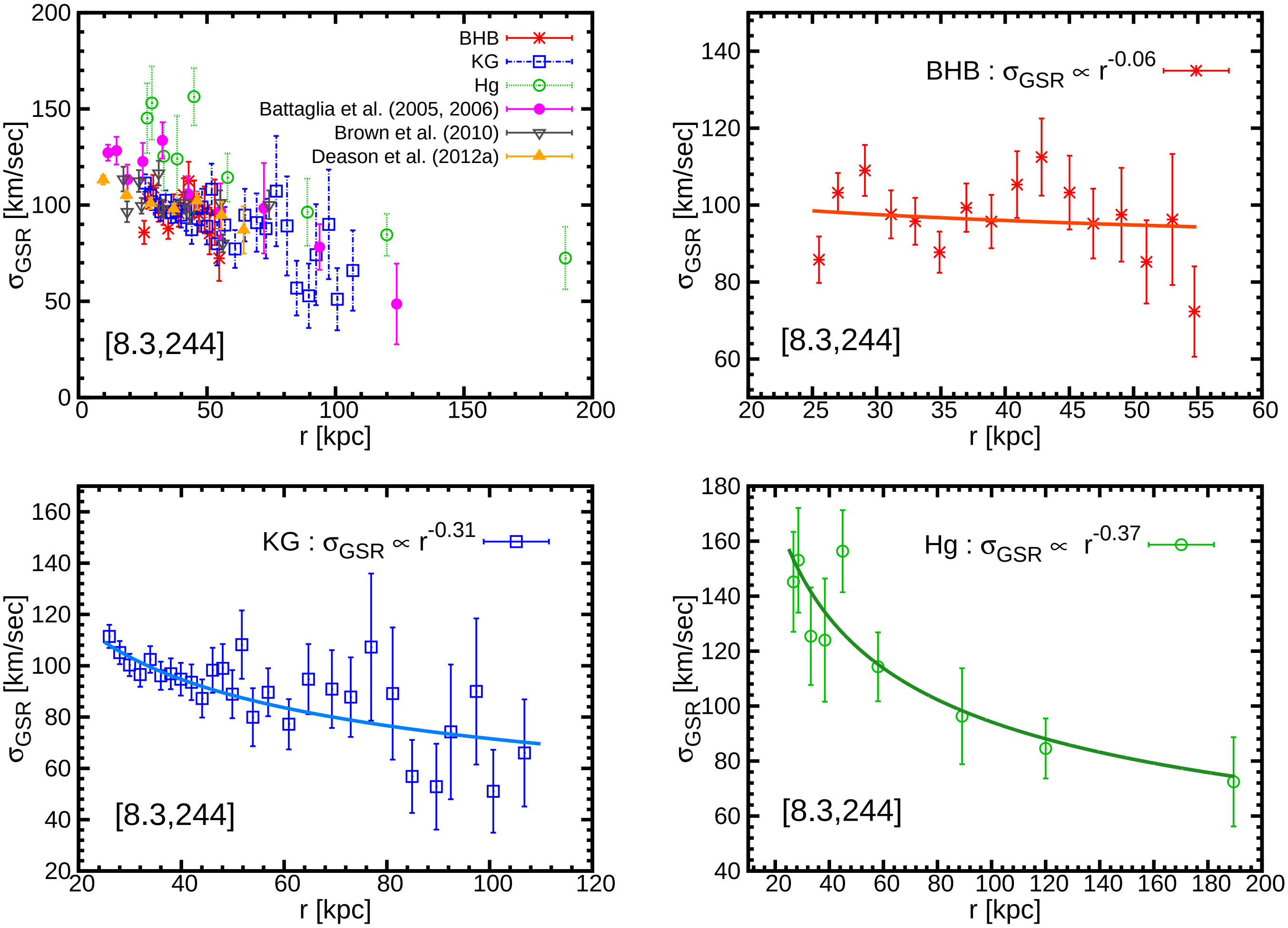

Fig. 7.— The GSR frame *los* velocity dispersion of the tracers, $\sigma_{\rm GSR}$, for the three non-disk tracer samples considered in this paper (see text and Figure 5 for details and source references for the samples). The top left panel also shows, for comparison, the $\sigma_{\rm GSR}$ obtained in some earlier studies (Battaglia et al. 2005, 2006; Brown et al. 2010; Deason et al. 2012a) which used different tracer samples. The other three panels show the best power-law fits to the radial profiles of $\sigma_{\rm GSR}$ for the three non-disk samples. The GC set used is $\left[\frac{R_0}{\rm kpc}, \frac{V_0}{\rm km\,s^{-1}}\right] = [8.3, 244]$.

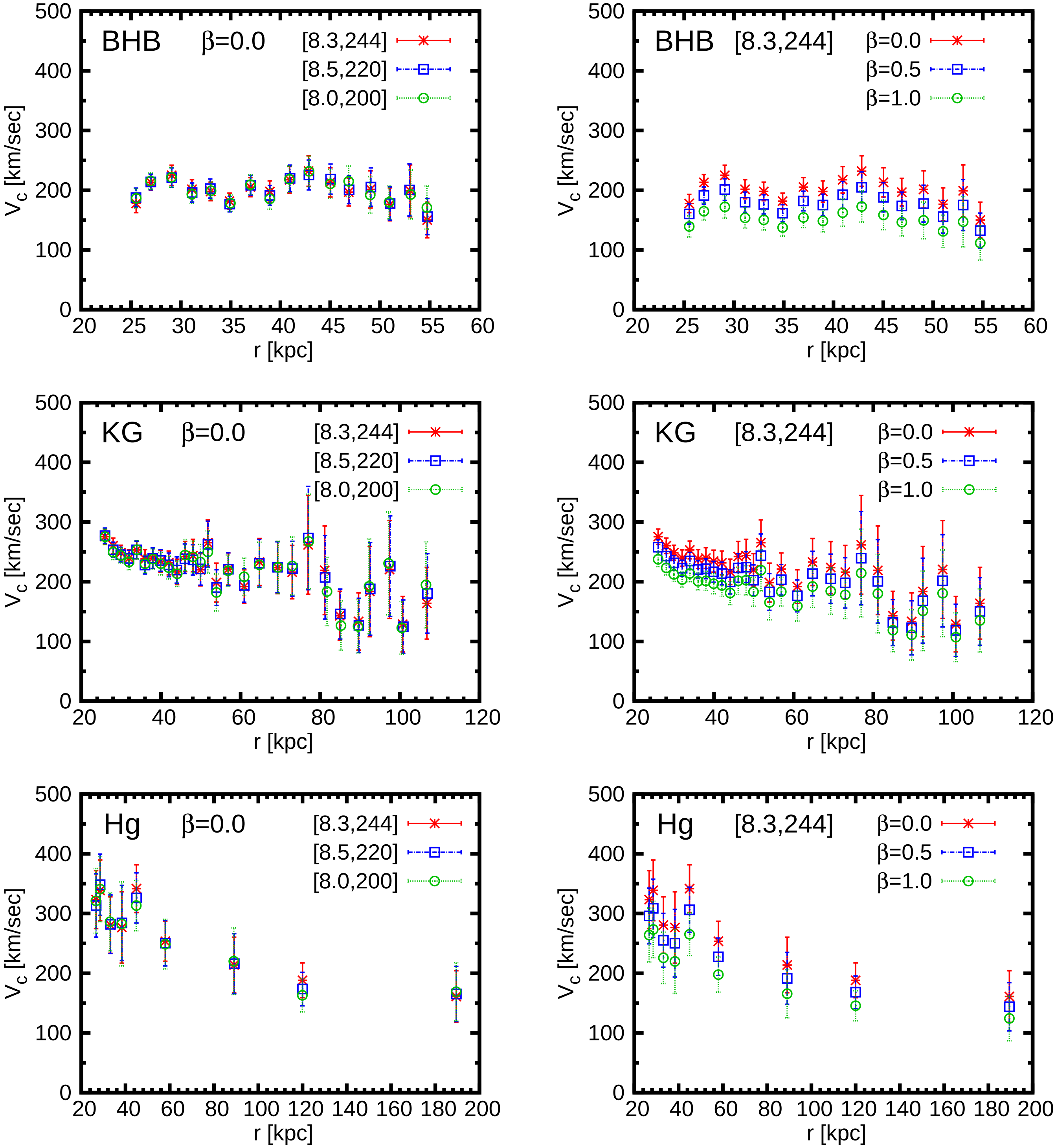

Fig. 8.— Circular velocities with their 1σ error bars for the three different non-disk tracer samples used in this paper (see text and Figure 5 for details and source references for the samples). The left panels are for tracer velocity anisotropy $\beta = 0$ and three different sets of values of the Galactic constants, $\left[\frac{R_0}{\rm kpc}, \frac{V_0}{\rm km\,s^{-1}}\right]$, as indicated, whereas the right panels show the results for three different constant (r-independent) values of $\beta = 0$, 0.5 and 1, with $\left[\frac{R_0}{\rm kpc}, \frac{V_0}{\rm km\,s^{-1}}\right] = [8.3, 244]$.

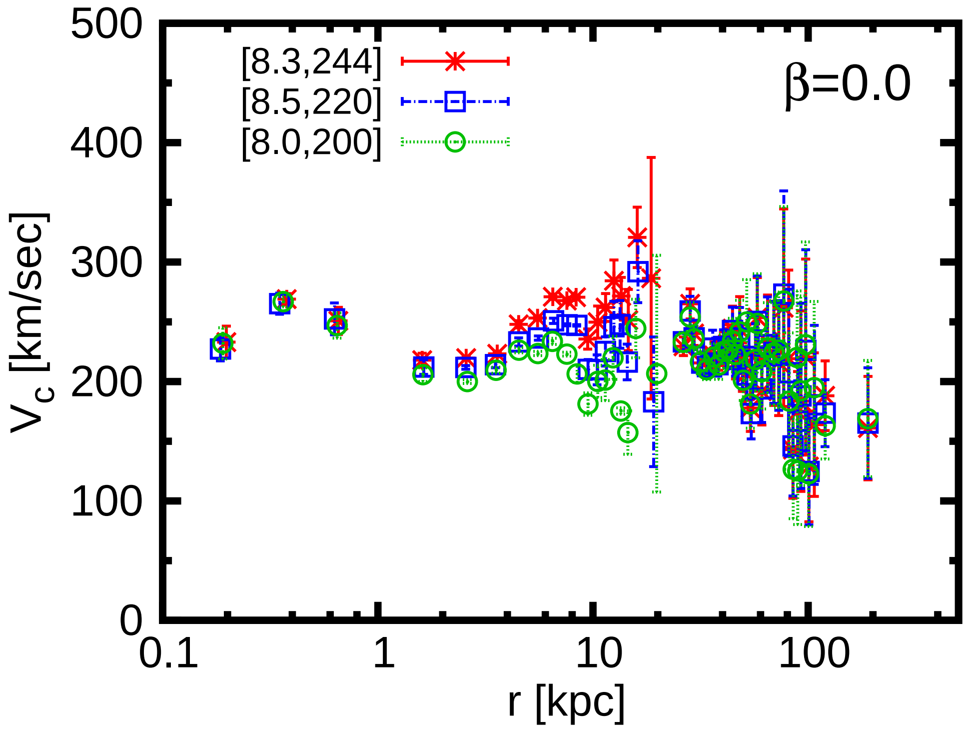

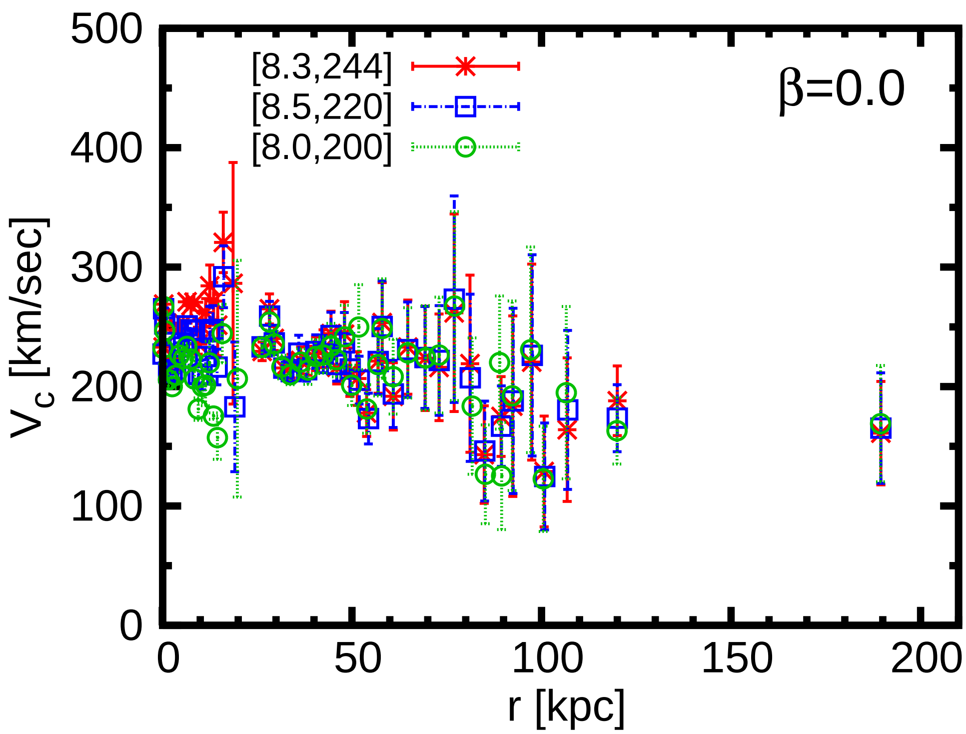

Fig. 9.— Top: Rotation curve of the Galaxy for three different sets of values of the Galactic constants $\left[\frac{R_0}{\text{kpc}}, \frac{V_0}{\text{km s}^{-1}}\right]$ as indicated and non-disk tracers' velocity anisotropy parameter $\beta = 0$. The data points and their 1σ error bars shown here are obtained by weighted averaging over the combined V_c data obtained from different disk and non-disk tracer samples (see Figures 4 and 8). Bottom: Same as above, but r in linear scale.

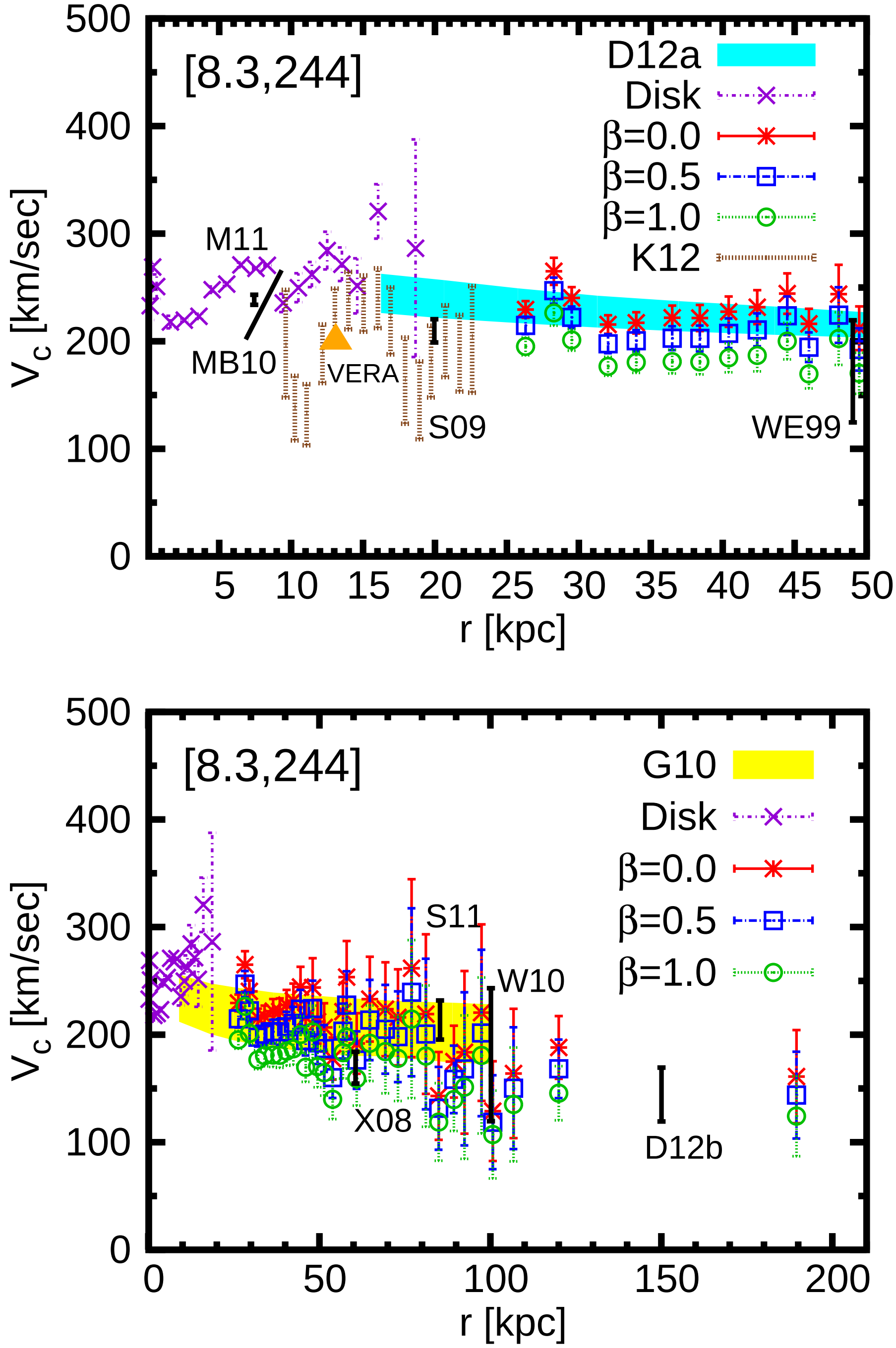

Fig. 10.— Rotation Curve for $\left[\frac{R_0}{\mathrm{kpc}}, \frac{V_0}{\mathrm{km\,s^{-1}}}\right] = [8.3, 244]$ and various values of β. The shaded bands marked D12a and G10 in the top and bottom panels, respectively, represent the RCs and their uncertainty bands obtained earlier by Deason et al. (2012a) (D12a) (up to $r \sim 50\,\mathrm{kpc}$) and Gnedin et al. (2010) (G10) (up to $r \sim 100\,\mathrm{kpc}$), respectively. In addition, some benchmark ranges of circular velocities at certain specific values of r obtained from various independent considerations by Kafle et al. (2012) (K12), Honma et al. (2007) (VERA), McMillan (2011) (M11), McMillan & Binney (2010) (MB10), Sofue et al. (2009) (S09), Wilkinson & Evans (1999) (WE99), Xue et al. (2008) (X08), Samurovic et al. (2011) (S11), Watkins et al. (2010) (W10), and Deason et al. (2012b) (D12b) are shown for comparison.

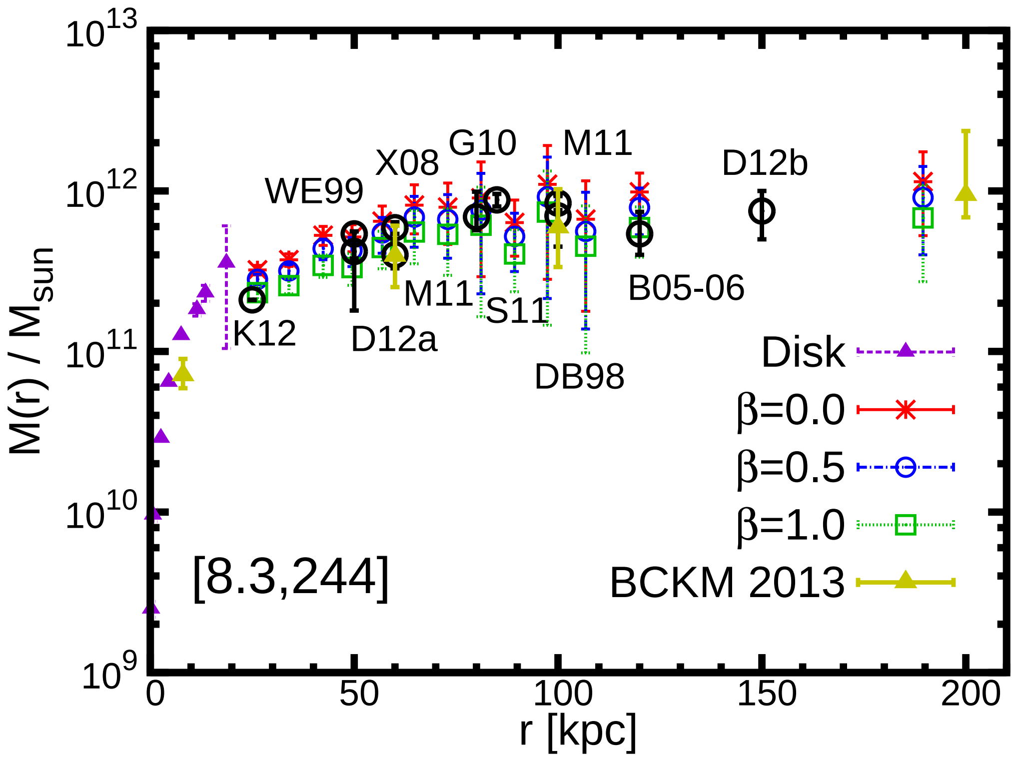

Fig. 11.— The mass, $M(r) = rV_c^2(r)/G$, within r, as a function of r, obtained from the RCs shown in Figure 10 for $\left[\frac{R_0}{\text{kpc}}, \frac{V_0}{\text{km s}^{-1}}\right] = [8.3, 244]$ and various values of the tracers' velocity anisotropy parameter β. Benchmark ranges of $M(r)$ at certain specific values of r obtained from various independent considerations in earlier works, namely, Kafle et al. (2012) (K12), Wilkinson & Evans (1999) (WE99), Deason et al. (2012a) (D12a), Xue et al. (2008) (X08), McMillan (2011) (M11), Gnedin et al. (2010) (G10), Samurovic et al. (2011) (S11), Dehnen & Binney (1998) (DB98), Battaglia et al. (2005, 2006) (B05-06), Deason et al. (2012b) (D12b), and Bhattacharjee et al. (2013) (BCKM 2013), are shown for comparison.

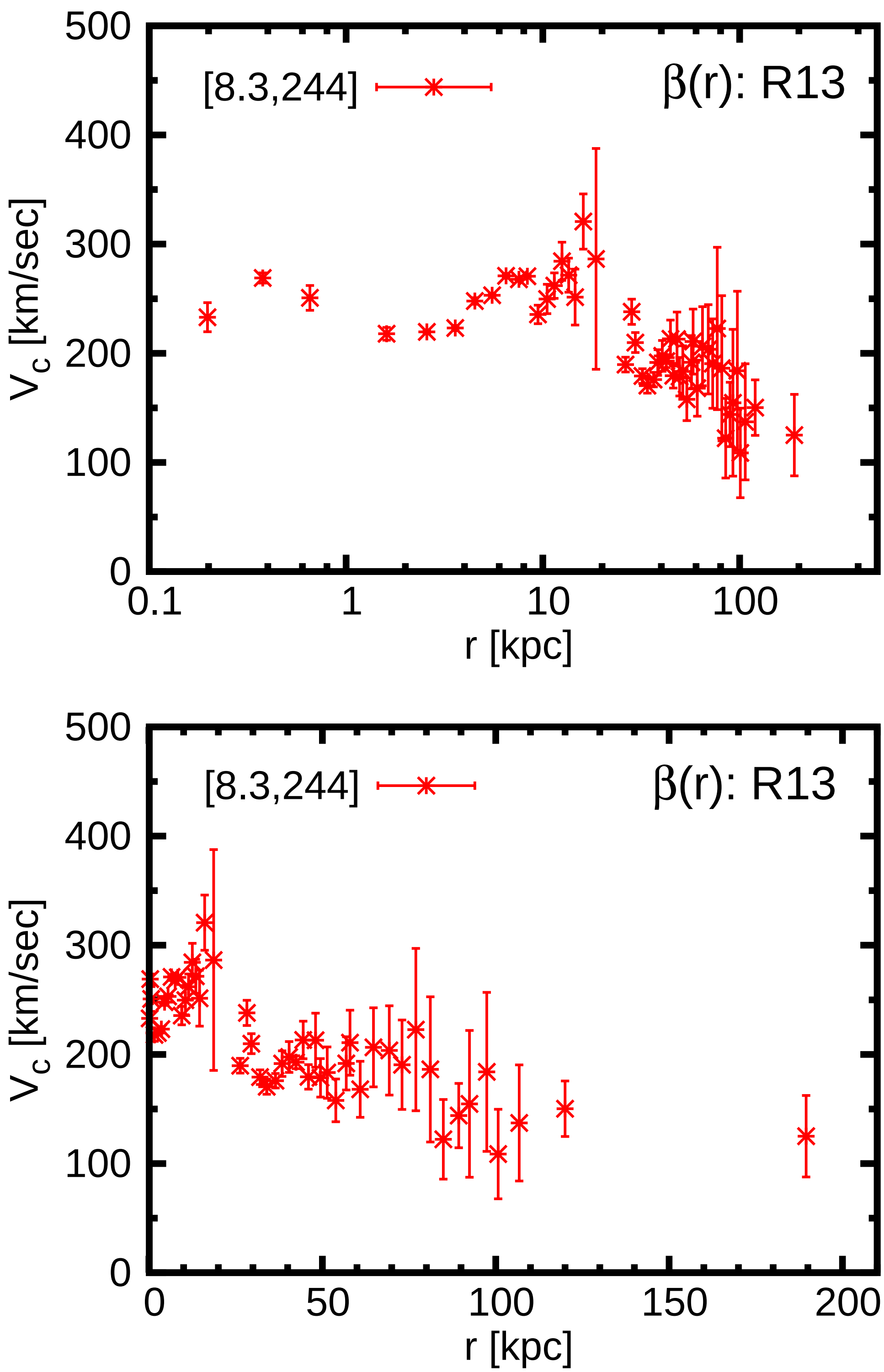

Fig. 12.— Top: Rotation curve of the Milky Way to $\sim 200\,\mathrm{kpc}$ for $\left[\frac{R_0}{\mathrm{kpc}}, \frac{V_0}{\mathrm{km\,s^{-1}}}\right] = [8.3, 244]$ and for a radial profile of the non-disk tracers' velocity anisotropy parameter β derived from Figure 2 of Rashkov et al. (2013) (R13). Bottom: Same as above, but with r in linear scale. The V_c data in numerical tabular forms for different sets of values of $\left[\frac{R_0}{\mathrm{kpc}}, \frac{V_0}{\mathrm{km\,s^{-1}}}\right]$ are available upon request from the authors.

Table 2: Best-fit parameter values for power-law fits to the radial profiles of the number density, $n_{\rm tr}$, and the Galactic Standard of Rest (GSR) frame *los* velocity dispersion, $\sigma_{\rm GSR}$, of the tracers for the three non-disk tracer samples considered in this paper (see text and Figure 5 for details and source references for the samples). The parameter values are given for three different sets of values of the GCs, $\left[\frac{R_0}{\rm kpc}\,,\,\frac{V_0}{\rm km\,s^{-1}}\right]$.

$\left[\frac{R_0}{\rm kpc}\,,\,\frac{V_0}{\rm km\,s^{-1}}\right]$	Number densities and radial velocity dispersions of non-disk tracers $n_{\rm tr}=n_0\,(\frac{r}{50\,{\rm kpc}})^{-\gamma}\,,\ \sigma_{\rm GSR}=\sigma_0\,(\frac{r}{50\,{\rm kpc}})^{-\alpha}$			
	$\frac{n_0}{\rm kpc^3}$	γ	$\frac{\sigma_0}{\rm km\,s^{-1}}$	α
	BHB			
$[8.3, 244]$	7.51×10^{-4}	4.16	93.0	0.06
$[8.5, 220]$	7.66×10^{-4}	4.15	94.45	0.07
$[8.0, 200]$	7.45×10^{-4}	4.17	93.58	0.05
	KG			
$[8.3, 244]$	6.57×10^{-4}	5.51	86.75	0.31
$[8.5, 220]$	6.53×10^{-4}	5.51	88.23	0.30
$[8.0, 200]$	6.40×10^{-4}	5.51	87.89	0.29
	Hg			
$[8.3, 244]$	2.37×10^{-5}	4.18	121.21	0.37
$[8.5, 220]$	2.39×10^{-5}	4.18	117.51	0.40
$[8.0, 200]$	2.38×10^{-5}	4.17	115.34	0.42